Progress In Electromagnetics Research C, Vol. 56, 1–13, 2015

Development of an Equivalent Circuit Model of a Finite Ground Coplanar Waveguide Interconnect in MIS System for Ultra-Broadband Monolithic ICs

Md Amimul Ehsan[2], Zhen Zhou[1], and Yang Yi[2, *]

Abstract—An equivalent circuit model of a finite ground plane coplanar waveguide (FGCPW) interconnect in a metal-insulator-semiconductor (MIS) system for an ultra-broadband monolithic IC is proposed and illustrated. An effective substrate considering Maxwell-Wagner Polarization is suggested and demonstrated. The method of modeling the weak skin effect of the conductor is presented. The accuracy of the equivalent circuit model is evaluated. This proposed FGCPW interconnect equivalent circuit model enables a quick and efficient time domain simulation to estimate the time delay and bandwidth of ultra-broadband ICs.

1. INTRODUCTION

The data rate which an ultra-broadband IC can actually support depends on its on-chip interconnects. Considerable research efforts have been expended to develop methods to rapidly and accurately model and characterize various on-chip interconnects [1–6]. For a data rate of 28 Gbps or higher, the interconnect impact becomes even more appreciable and needs to be modeled appropriately. For example, the frequency response of a high-speed photo-detector (PD) is determined by the transit time, junction resistance, and capacitance; the response must also include interconnect induced parasitic effects between the PD and receiver circuitry.

A FGCPW on MIS, as depicted within Figure 1, often serves as the interconnection between the PD and an external receiver circuitry such the trans-impedance amplifier (TIA). Historically, a full wave solver such as HFSS [7] is employed to simulate the FGCPW within the frequency domain; the resulted S-parameters are then used for circuit transient simulation and AC simulation. HFSS simulation can be extremely costly in computational time and memory overhead for complex structures with high aspect ratios. Accurately modeling such interconnects at a reasonable computation cost has been a very active research field. For example the work presented in [8–10] demonstrate the extension of the Foldy-Lax multiple scattering approach toward modeling the multivia in a layered dielectric substrate; the accuracy of the results are comparable to HFSS simulations, but at a fraction of the cost.

The transverse dimensions of the interconnects shown in Figure 1 are smaller than 1e-5 of the guided wavelength at frequencies lower than 1 GHz; for such instances, utilizing HFSS to obtain accurate passive solutions is problematic. When the S-parameter or equivalent circuit model created by HFSS is explicitly used in a transient simulation, the DC condition of the PD will be inaccurately predicted, along with the DC bias condition of TIA. Aside from the DC inaccuracy, the HFSS simulation time is intensive. Whereas, an equivalent circuit model offers both realistic DC conditions and a rapid assessment of the interconnect bandwidth. Most importantly, the equivalent circuit model can be used to optimize PD design towards optimizing bandwidth.

Received 8 October 2014, Accepted 15 December 2014, Scheduled 29 January 2015
* Corresponding author: Yang Yi (yyi@ku.edu).
[1] Intel Corp., 3600 Juliette Ln, Santa Clara, CA 95054, USA. [2] Department of Electrical Engineering and Computer Science, University of Kansas, Lawrence, KS 64110, USA.

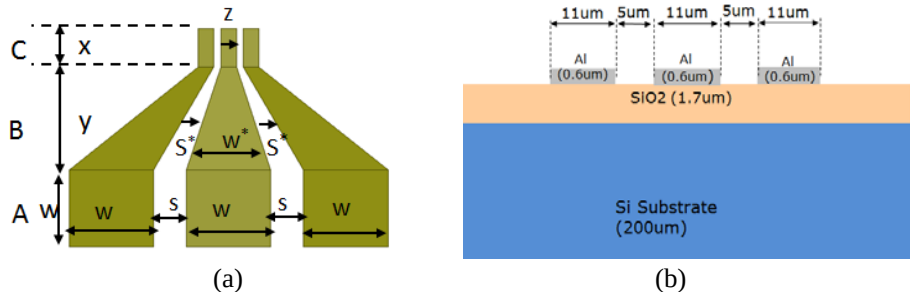

Figure 1. The FGCPW interconnect ($w = 60\,\mu\text{m}$, $s = 23\,\mu\text{m}$, $y = 200\,\mu\text{m}$, $x = 25\,\mu\text{m}$, $z = 11$, w^* varies from 60 µm at the bottom to 11 µm at the top, while s^* varies from 23 µm at the bottom to 5 µm at the top within region B, gap in C section is 5 µm). (a) Top view. (b) Cross section.

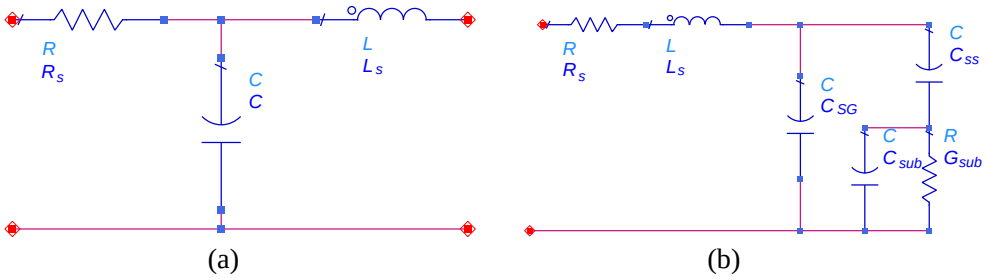

Figure 2. Lumped element model for the FGCPW interconnect. (a) Conventional model. (b) Equivalent circuit model proposed in [2].

An equivalent circuit as shown on Figure 2(a) is often used to model interconnects, where R_s, L_s, and C_{pad} are the series resistance, series inductance, and pad capacitance, respectively. The lumped elements in Figure 2(a) are regarded as frequency independent components; they are typically characterized by LRC measurements obtained at low frequency. The bandwidth of the interconnect is calculated merely by using a single-pole RC model formed by R_s and C_{pad}, assuming L_s is negligible. This simplification is valid only when the data rate is low, the silicon resistivity is very high, and the interconnect length and transverse dimension is much smaller than the guided wavelength. For the interconnect studied in this work, the frequency range of interest is 0.1 GHz to 40 GHz, the resistivity of Si substrate is 100 Ω-cm, and the interconnect is 312 µm long; as a consequence the voltage and current vary in magnitude and phase over the entire length; thus the equivalent circuit model shown in Figure 2(a) becomes inappropriate.

Depending on the operating frequency and the resistivity of the silicon substrate, at least two possible modes can propagate in a MIS system: the dielectric Quasi-TEM mode, and the Slow-wave mode [11, 12]. Generally, either mode can be described by its corresponding equivalent circuit. Shibata and Sano proposed the use of a single RLGC model as presented in Figure 2(b) to describe both Quasi-TEM and Slow-wave mode propagations for certain ranges of substrate resistivity [12]. All parameters in Figure 2(b) are assumed frequency independent. The assumption of frequency independence of the RLGC model may be erroneous.

To this extent, Milanović et al. [1] expanded the work related in [12] to include the frequency dependence of the RLGC. R and L are calculated from a technique of "phenomenological equivalent loss method", or PEM [13]. However, PEM may unrealistically estimate R and L whenever the one-dimension skin depth based recession results in negative or very narrow signal or ground plane widths. Moreover, the geometrical parameter estimation is simply not accurate enough. The extracted $R(\omega)$ in [1] is much lower than the measured; as a consequence, an additional R_l corrective term must be added to match the observation. But the existence of R_l requires the presence of longitude electrical field in the silicon substrate that increases with frequency linearly, which in turn contradicts the assumption of Quasi-TEM mode propagation in the silicon substrate.

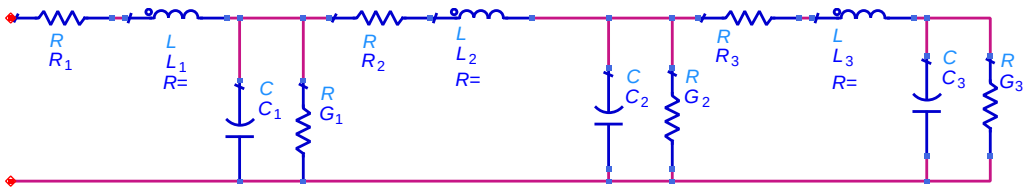

Figure 3. Cascaded lumped element model for the FGCPW interconnect.

Considering accurately model the R and L in the equivalent circuit, Tran et al. [2] proposed a classical RLGC equivalent circuit to describe CPW in MIS behavior, by extracting RLCG effects from the measurement. To have the extractions match the models in R and L, additional elements were added to the serial terms of the model to account for the eddy currents in the conductive substrate and conductor. As related in [2], the parameters accounting for the eddy current do not have any intrinsic physical meaning. Besides the R and L, the capacitance C is modeled as the Si substrate capacitance in parallel with the capacitance of the SiO_2 layer.

Then regarding the TEM wave propagating within the interconnect, a frequency dependent RLGC model should be entirely adequate to describe the propagation. In this paper, a simple equivalent circuit model shown in Figure 3 is proposed to supersede the interconnect presented within Figure 1. In order to calculate the frequency dependent C and G of the equivalent circuit under different propagation modes, this paper introduces a concept of an equivalent substrate which captures the Maxwell-Wagner interfacial polarization. This paper then evaluates the frequency dependent R and L for conditions wherein an assumption of shallow field penetration within the conductor does not apply.

The results of this paper are organized as follows: Section 2 presents the equivalent substrate calculation and RLGC calculation. In Section 3, the accuracies of the RLGC extractions are evaluated against their corresponding Ansoft Q3D extractions; then the equivalent circuit predicted S-parameter is compared to the HFSS simulation at a frequency higher than 1 GHz. Then the accuracy of the equivalent circuit is examined by comparing it to the measurement for an open ended structure shown in Figure 1(a). Conclusions and alternative mechanisms that limitFGCPW bandwidth are discussed within Section 4.

2. EQUIVALENT CIRCUIT MODEL PARAMETER CALCULATIONS

2.1. Effective Substrate of MIS

Maxwell-Wagner interfacial polarization in the MIS structure induces slow-wave propagation. For the FGCPW interconnect concerned within this work, the wave propagates either in slow wave mode, dielectric Quasi-TEM mode, or in the transition between these two modes. The simplest way to describe both modes is to introduce a single effective substrate with an effective dielectric permittivity described by a single-pole Debye model, as related in [11, 14]:

$$\varepsilon_{er} = \varepsilon_{e\infty} + \frac{\varepsilon_{es} - \varepsilon e_{\infty}}{1 + j\omega\tau_e} = \varepsilon'_{er} - j\varepsilon''_{er} \tag{1}$$

where ε_{es} and $\varepsilon_{e\infty}$ are the static permittivity and the optical permittivity of the effective substrate, τ is its relaxation time, and σ_e is its equivalent conductivity.

Following the analysis in [11], $\varepsilon_{e\infty}$ can be simply set to be ε_{si}. Then the dielectric relaxation time τ_e equals:

$$\tau_e = \frac{1}{2\pi}\left(\frac{1}{f_e} + \frac{1}{f_s}\right) \tag{2}$$

where f_e is Si substrate dielectric relaxation frequency:

$$f_e \equiv \frac{\sigma_{si}}{2\pi\varepsilon_0\varepsilon_{si}} \tag{3}$$

For this work, $f_e = 1.512$ GHz, and f_s is the relaxation frequency of interfacial polarization at which ε''_{er} is half of ε_{es}.

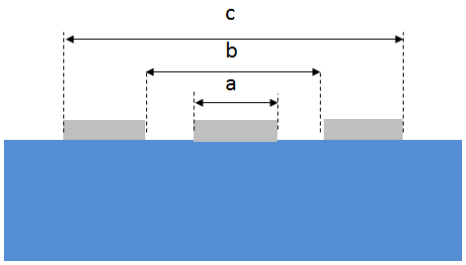

Figure 4. The FGCPW cross section.

Table 1. Parameters of Debye model of equivalent substrate.

Segment	ε_{es}	$\varepsilon_{e\infty}$	τ_e second
A	59	11.9	6.3131e-10
B	39.12	11.9	3.1566e-10
C	26	11.9	3.1566e-10

Depending on the differential between $\varepsilon_{e\infty}$ and ε_{es}, setting ε''_{er} to half of ε_{es} may not always result in a feasible solution for f_s. We propose setting f_s to be half of f_e whenever equating ε''_{er} to be half of ε_{es} is not feasible. Subsequent results, as will be presented below, indicate the above proposition is verified.

The permittivity of the effective substrate will vary its static value ε_{es} to its optical value of $\varepsilon_{e\infty} = \varepsilon_{Si}$. ε_{es} can be estimated as:

$$\varepsilon_{es} = \frac{C_{ox}}{2\varepsilon_0} \frac{K(k)}{K(k')} + 1 \tag{4}$$

K is the complete elliptical integral of first kind. Referring to Figure 4, the module k and k' are given by Equation (5) or Equation (6) [15].

$$k = \frac{\sinh(\pi a/d)}{\sinh(\pi b/d)} \sqrt{\frac{\sinh^2(\pi b/d) - \sinh^2(\pi a/d)}{\sinh^2(\pi c/d) - \sinh^2(\pi b/d)}} \quad (c < d) \tag{5a}$$

$$k = \frac{\sinh(\pi a/d)}{\sinh(\pi b/d)} \quad (c \geq d) \tag{5b}$$

$$k' = \sqrt{1 - k^2} \tag{6}$$

And

$$C_{ox} = \varepsilon_{ox} \left(\frac{a}{t_{ox}}\right) + 1.5\varepsilon_{ox} \left(\frac{a}{t_{ox}}\right)^{0.1} \tag{7}$$

where t_{ox} is the SiO_2 layer thickness, and ε_{ox} is the dielectric permittivity of SiO_2 [1].

The effective substrate parameters for segments A, B, and C are listed below within in Table 1.

2.2. Equivalent Circuit Model Parameter Calculations

2.2.1. Line Capacitance C and Conductance G Calculations

The total capacitance per unit length of the FGCPW is the sum of the partial capacitance C_0 and C_1:

$$C = C_0 + C_1 \tag{8}$$

where C_0 is the partial capacitance of the FGCPW in the absence of the dielectric layers given by Equation (9) [1].

$$C_0 = 4\varepsilon_0 \left(\frac{K(k'_0)}{K(k_0)} + \frac{t}{(b-a)}\right) \tag{9}$$

Referring to Figure 4, the modules of the complete elliptic integral of the first kind are given by Equations (10) and (11) [15]:

$$k_0 = \frac{c}{b}\sqrt{\frac{b^2 - a^2}{c^2 - b^2}} \quad (c < d) \tag{10a}$$

$$k_0 = \frac{a}{b} \quad (c \geq d) \tag{10b}$$

$$vk_0' = \sqrt{1 - k_0^2} \tag{11}$$

C_1 (Equation (8)) is the partial capacitance of the FGCPW with only the equivalent substrate, and is determined as [15]:

$$C_1 = 2\varepsilon_0 \left(\varepsilon_{er}' - 1\right) \frac{K\left(k'\right)}{K\left(k\right)} \tag{12}$$

where k and k' were defined by Equations (5) and (6).

The conductance per unit length of the FGCPW is related to its substrate partial capacitance as

$$G = \omega C_1 \tan\delta \tag{13}$$

where ω is the angle frequency, and $\tan\delta$ is the loss tangent of the equivalent substrate.

2.2.2. Line Resistance R and inductance L Calculations

Conventionally, the frequency dependent line resistance R_{ac} is derived from Wheelers incremental inductance rule as [13]:

$$R_{ac} = \frac{R_s}{\mu_0} G \tag{14}$$

where R_s is the surface resistance:

$$R_s = \frac{1}{\sigma\delta_s} \tag{15}$$

and G is a geometric factor in a form of

$$G = \frac{1}{\mu_0} \sum_j \frac{\partial L_{e\infty}}{\partial n} \tag{16}$$

The $\partial L_{e\infty}/\partial n$ is the derivative of the external inductance with respect to the incremental recession of the conductor wall j; whereas $L_{e\infty}$, the external inductance, is related to C_0 as:

$$L_{e\infty} = \frac{1}{c^2 C_0} \tag{17}$$

L_{int} is related to R_{ac} as

$$L_{int} = \frac{R_{ac}}{\omega} \tag{18}$$

The Wheelers incremental inductance rules assume shallow penetration which is true only under the condition that the conductor thickness is at least a few skin depths. When the assumption is no longer valid, the inductance incremental rule fails to accurately predict R_{ac} and L_{int}. To account for the field penetration effect for a thin conductor, Lee and Itoh proposed a phenomenological loss equivalent method (PEM) to calculate R_{ac} and L_{int} with a correction factor on surface resistance for finite strip thickness as [13]:

$$Z_s^t = Z_s \coth\left(\sqrt{j\omega\mu\sigma}\, t\right) \tag{19}$$

where t is the conductor thickness and Z_s the surface impedance given as $Z_s = (1 + j)R_s$. With this correction, the internal impedance due to the finite conductance becomes:

$$Z_i = (1 + j)\, R_s G \coth\left[\frac{(1 + j)\, GA}{\delta_s}\right] \tag{20}$$

where A is the conductor area. Consequentially, the resistance per unit length due to the conductor loss can be derived as

$$R_{ac} = \mathrm{Re}\left(Z_{i,center} + Z_{i,gnd}\right) \tag{21}$$

The total resistance per unit length is

$$R = R_{dc} + R_{ac} \tag{22}$$

The total inductance per unit length can be expressed as

$$L = L_{\infty} + L_{int} = L_{\infty} + \mathrm{Im}\left(Z_{i,center} + Z_{i,gnd}\right) \tag{23}$$

For CPW and FGCPW, analytical solutions for C_0 are derived through conformal mapping in [16, 17]. Given a closed form for C_0, then R_{ac} and L_{int} can be calculated analytically as demonstrated in [17]. However, when the R_{ac} and L_{int} are calculated using PEM for the segments using Equations (14) to (23), the PEM values are significantly different than what Q3D predicts. For illustrative purposes, the PEM calculated R_{ac} and L are compared to Q3D extractions; the comparisons are presented in Figure 5. The discrepancy between PEM and Q3D extraction is significant, particularly at low frequency.

The accuracy of PEM principally depends on the accuracy of the G determination. Causes of the deflection of PEM at lower and higher frequency are well related in [13]. The remedy for improved accuracy is the utilization of a complex FEM (finite element model) to determine G. The purpose of this paper is to relate a simple equivalent circuit model for Matlab to calculate the G parameter; circumventing the necessity of the FEM.

The conductance of the aluminum considered in this work is $3.8e7\,\mathrm{S/m}$ and the conductor thickness is $0.6\,\mu\mathrm{m}$. At a frequency lower than $18.5\,\mathrm{GHz}$, the skin depth is greater than the conductor thickness. The resistance will remain at approximately the DC value until $18.5\,\mathrm{GHz}$, after which AC resistance effects begin to manifest. However, even at $40\,\mathrm{GHz}$, the skin depth is only 1.4 times the conductor thickness; hence the current is not completely confined within one skin depth. To account for the weak skin effect, segmentation models for R and L are proposed in [17] with a requirement that the signal width W_g is greater than the ground plane width W_c. For the interconnect studied in this work, $W_g = W_c$, hence the R and L models developed in [17] are not applicable.

However, the root-sum-square function such as Equation (24) can be used to take the weak skin effect into consideration [18]:

$$R = \sqrt{R_{dc}^2 + R_{ac}^2} \tag{24}$$

R_{ac} is related to the power loss per unit length as

$$P_l = \frac{\sigma}{2}\iint E \cdot E^* ds = \frac{|Z_s|^2}{2\sigma}\iint J_s J_s^* ds = \frac{1}{2} I_0^2 R_{ac} \tag{25}$$

where Z_s is again the surface impedance. The surface current J_s is related to the propagation coefficient inside the conductor γ and the penetration depth t_e as:

$$J_s = J_{s0} e^{-\gamma t_e} \tag{26}$$

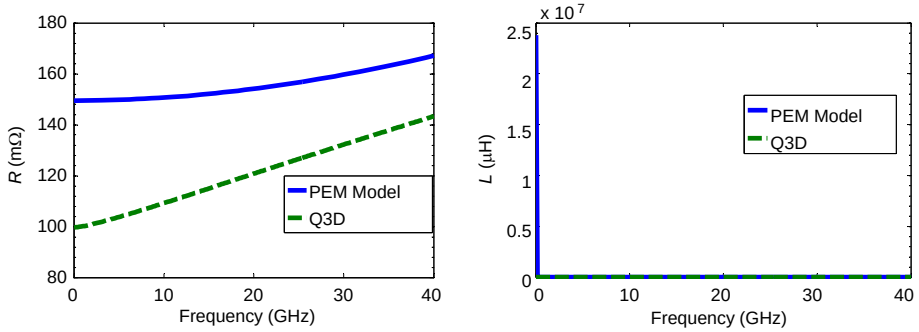

Figure 5. Comparison of extracted R and L for segment C with PEM and Q3D.

Then, using Equation (25) in conjunction with Equation (26), we can derive

$$R_{ac} = \frac{|Z_s|^2}{\sigma I_0^2} \int_0^t e^{-\gamma t_e} dt_e \oint J_s J_s^* dl = \frac{|Z_s|^2}{\sigma I_0^2} \left(1 - e^{-\gamma t}\right) \oint J_s J_s^* dl \tag{27}$$

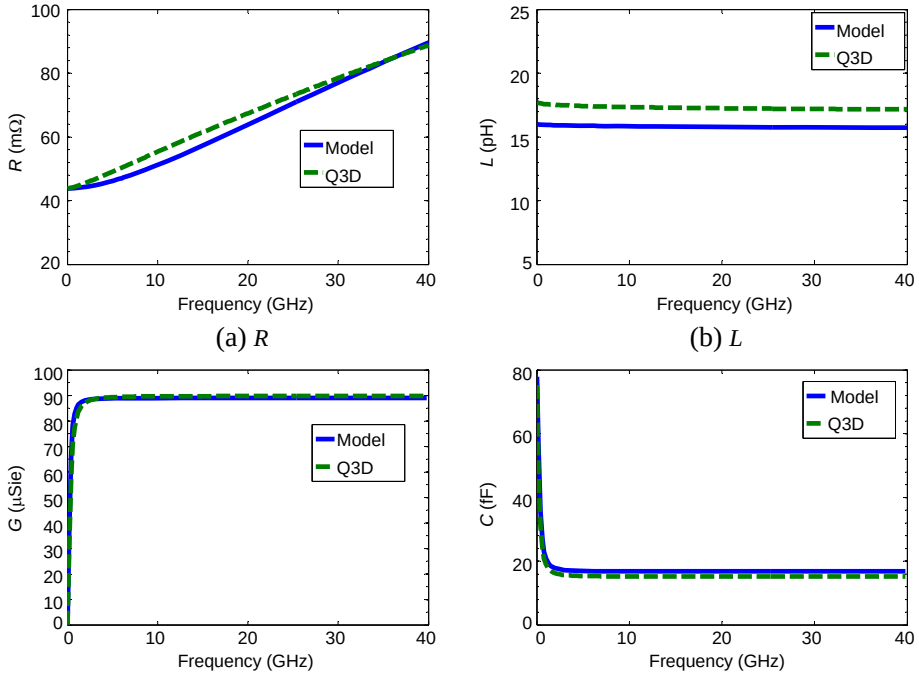

Figure 6. Segment A RLGC extraction comparisons.

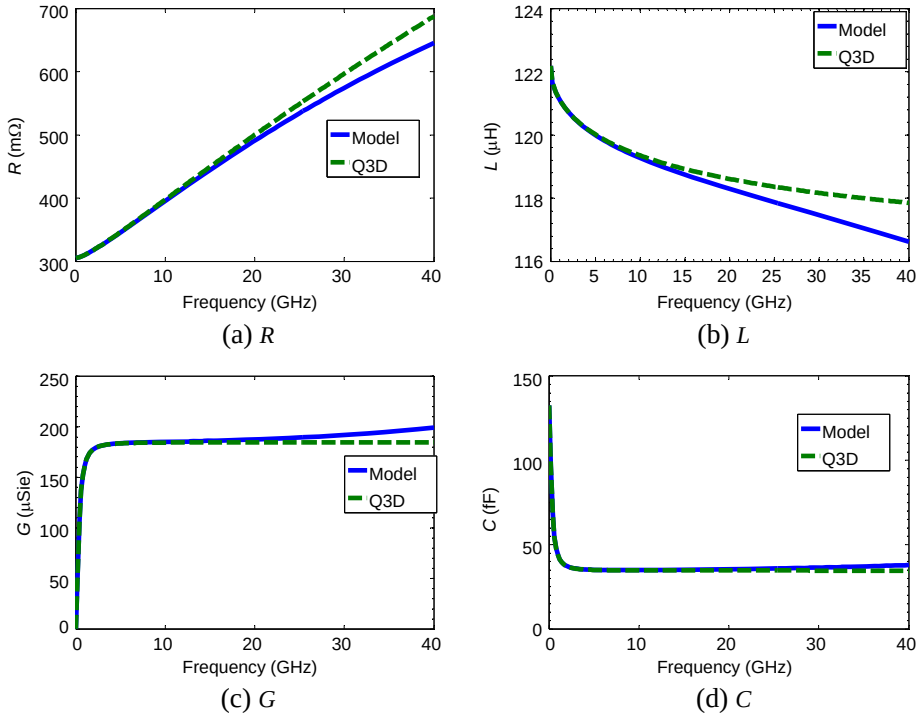

Figure 7. Segment B RLGC extraction comparisons.

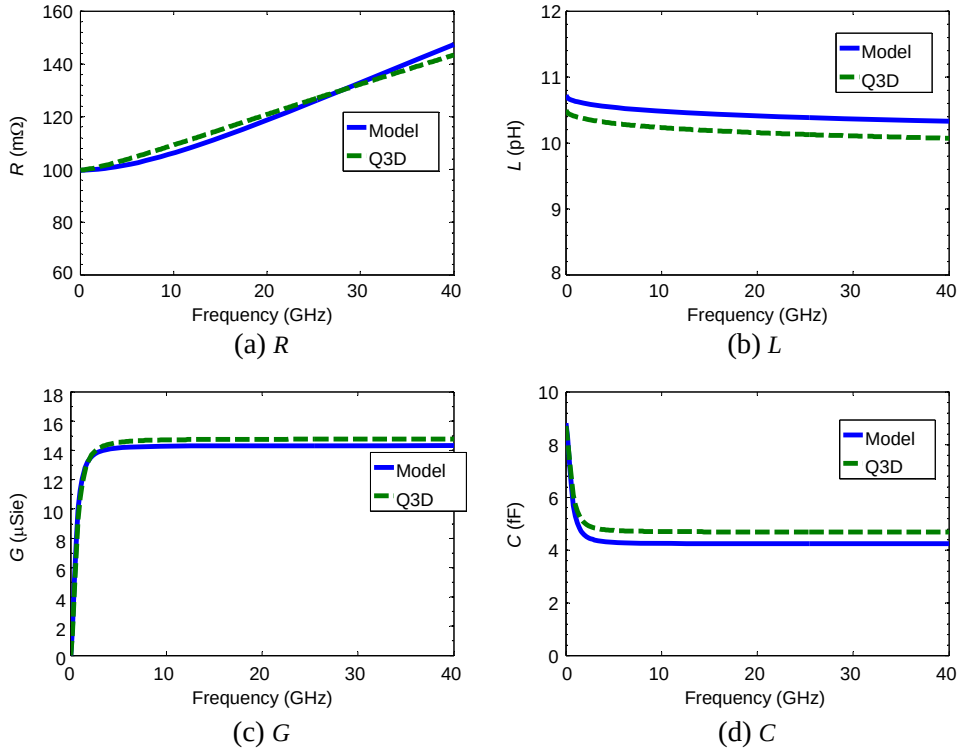

Figure 8. Segment C RLGC extraction comparisons.

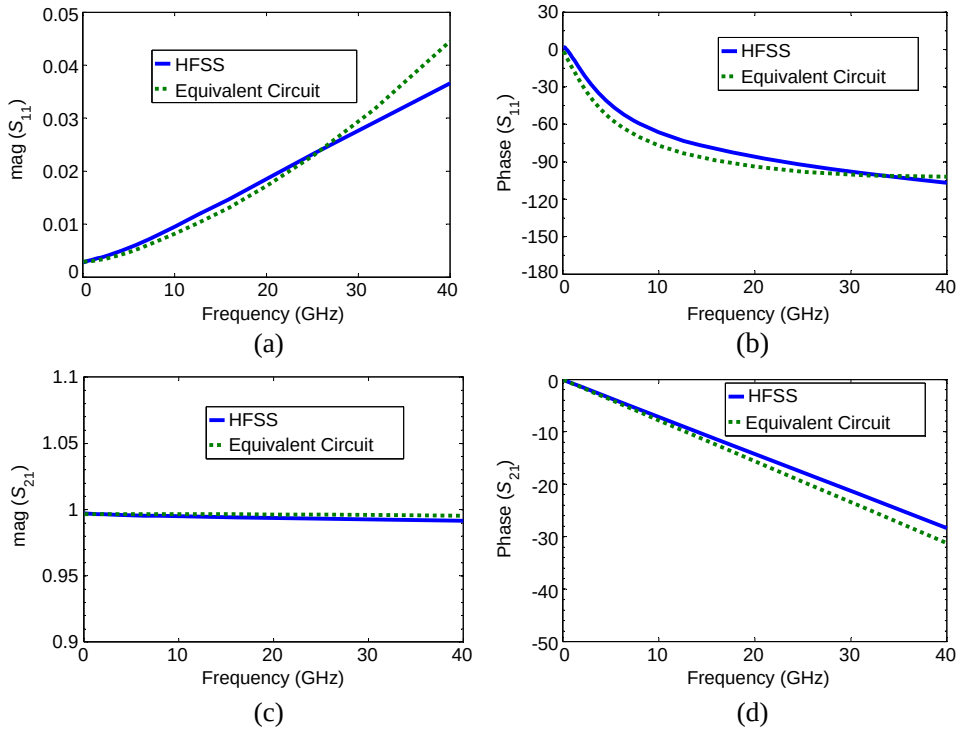

Figure 9. HFSS and equivalent circuit simulated S-parameters. (a) S_{11} magnitude. (b) S_{11} phase. (c) S_{21} magnitude. (d) S_{21} phase.

Assuming the current crowds towards the edges of the conductors as demonstrated in [16], the R_{ac} can be derived by using Equation (3.197) in [16] with a correction coefficient of $(1 - e^{-\gamma t})$. L_{int} can be calculated using Equation (18).

3. EQUIVALENT CIRCUIT MODEL PARAMETER EXTRACTION RESULTS AND COMPARISONS

Using the equivalent substrate and the closed-formed equations for RLGC, the equivalent circuit parameters for each segment are obtained and their values are compared to their corresponding Ansoft Q3D extractions. As demonstrated within Figures 6, 7, and 8, the calculated RLCG parameters are in good agreement with the Q3D extractions.

The S-parameters of the FGCPW interconnects studied for this work are calculated with the equivalent circuits illustrated in Figure 3, and are compared to their HFSS simulated values. As demonstrated in Figure 9, at up to 30 GHz, the simulated S-parameters using the equivalent circuit

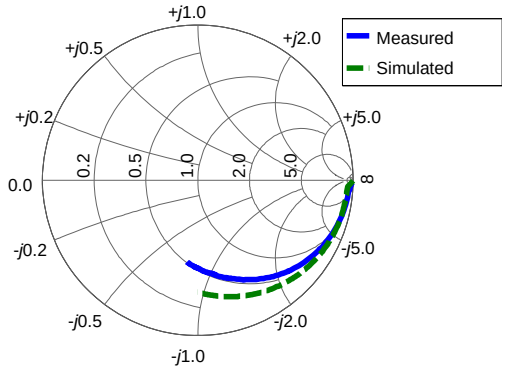

Figure 10. Measured and circuit model predicted S_{11}.

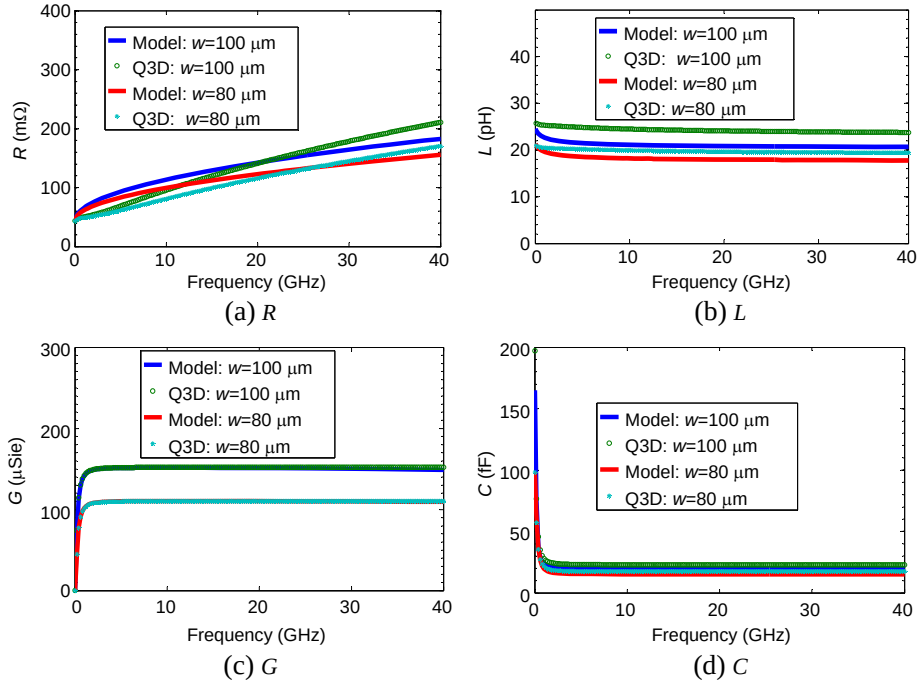

Figure 11. Segment A RLGC extraction comparisons ($w = 100\,\mu$m and $80\,\mu$m).

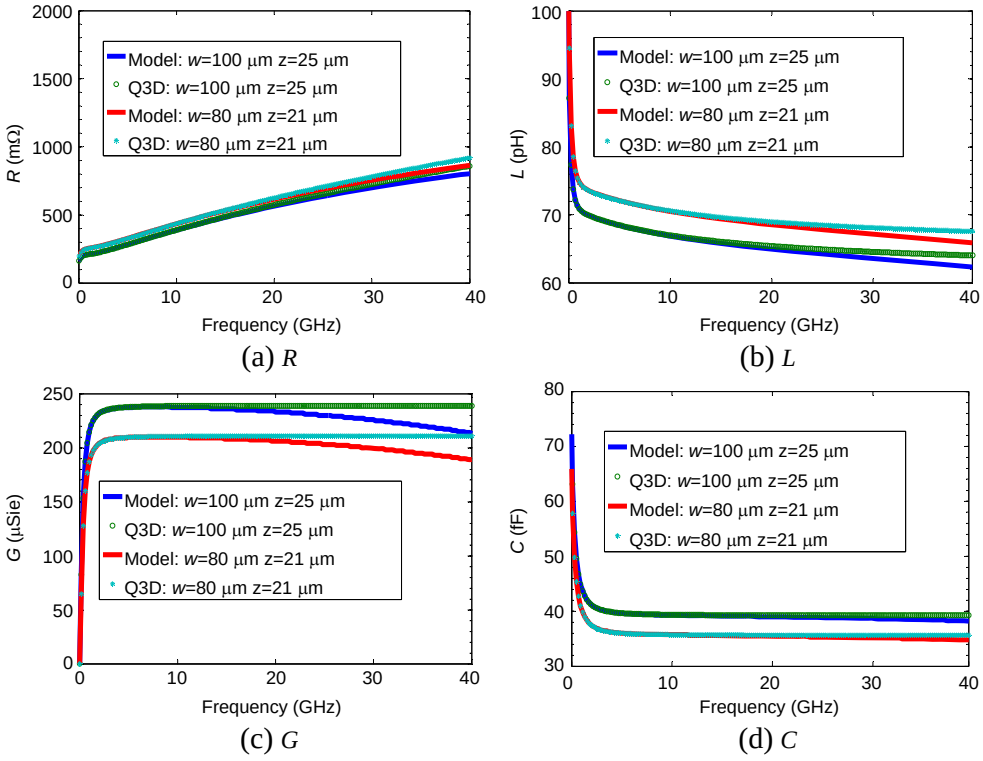

Figure 12. Segment B RLGC extraction comparisons ($w = 100\,\mu\text{m}$ and $80\,\mu\text{m}$; $z = 25\,\mu\text{m}$ and $21\,\mu\text{m}$).

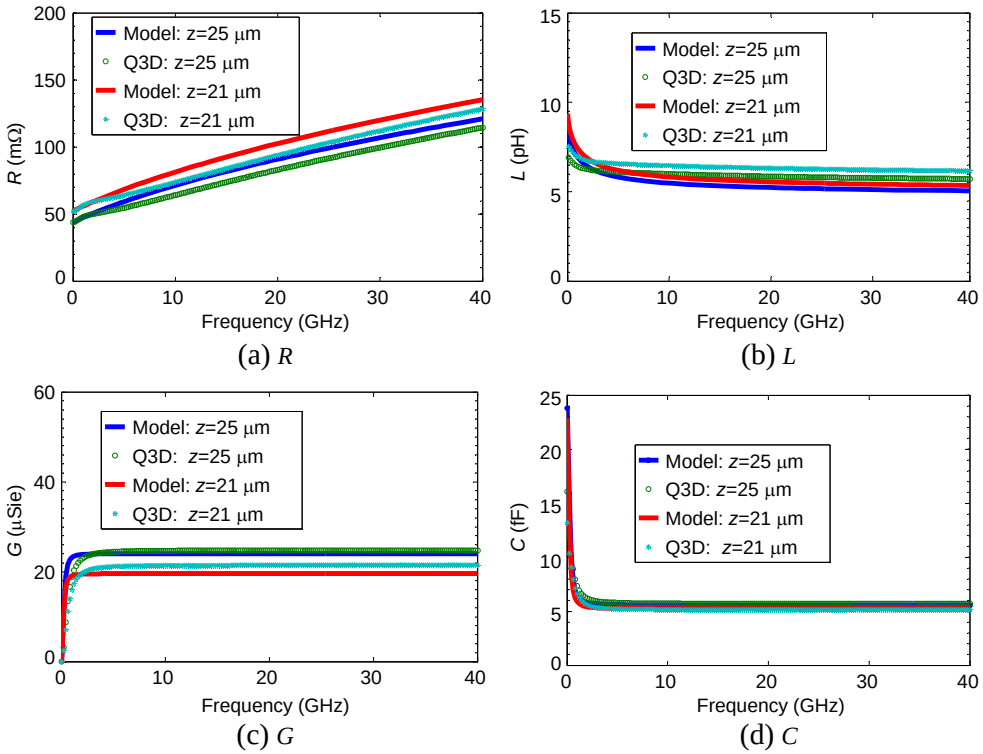

Figure 13. Segment B RLGC extraction comparisons ($z = 25\,\mu\text{m}$ and $21\,\mu\text{m}$).

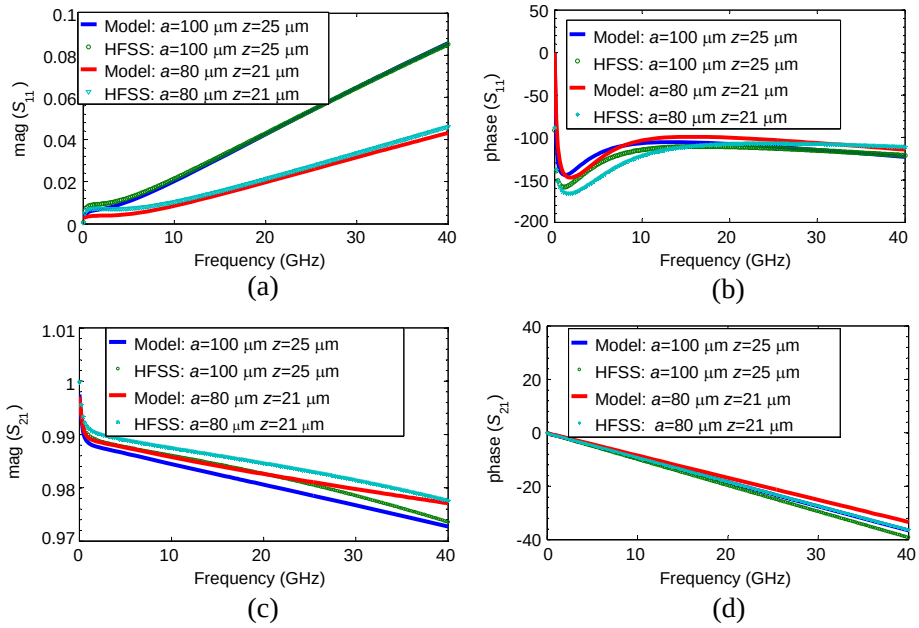

Figure 14. HFSS and equivalent circuit simulated S-parameters ($w = 100\,\mu\text{m}$ and $80\,\mu\text{m}$; $z = 25\,\mu\text{m}$ and $21\,\mu\text{m}$).

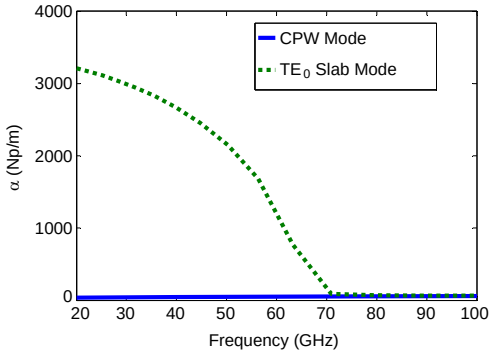

Figure 15. HFSS simulated α for CPW and TE_0 modes.

model are in good agreement with those determined by HFSS. Figure 10 shows the comparison between the measured and circuit model predicted S_{11}.

To further demonstrate the effectiveness of the methodology developed within this paper, two more cases with $w = 100\,\mu\text{m}$ and $80\,\mu\text{m}$, and $z = 25\,\mu\text{m}$ and $21\,\mu\text{m}$, respectively, as presented in Figure 1 were investigated. The equivalent circuit predicted RLGC for these cases were compared to Q3D extractions. As illustrated in Figures 11, 12, and 13, the equivalent circuit predictions are in good agreement with the Q3D extractions. Furthermore, the equivalent circuit predicted S-parameters for these two cases are examined by the similitude between the model prediction and the HFSS simulations as illustrated in Figure 14; and so despite of the crudity of the derivations, the model compares remarkably well to the simulation.

One port measurement, S_{11}, was performed on a fabricated metal interconnect with dimensions and cross-sections virtually identical to that illustrated in Figure 1, over the frequency range of 0.1 to 40 GHz with an Anritsu 40 GHz Vector Network Analyzer (VNA). An $85\,\mu\text{m}$ GSG probe from GGB was used to perform the measurement [19]. A SOLT (short, open, load, and transmission) calibration was performed using GGB calibration substrate. The measurement was taken by probing the pads shown as Segment A in Figure 1. The open response of the interconnect was simulated with the equivalent circuit

developed in this work. For the simulation, the contact resistances between the aluminum pad and the probe as well as the end effect caused by the probe skating on the pad are taken into consideration. The simulation result was compared to the measurement. And as illustrated within Figure 10, the equivalent circuit simulation using the extracted equivalent circuit parameter is in good agreement with the physical observation.

4. CONCLUSION AND DISCUSSION

In this work, we proposed a causal equivalent circuit for a FGCPW interconnect in MIS system that can be used for the transient simulation. We introduced a concept of an effective substrate to capture both slow wave and dielectric Quasi-TEM modes, and developed a method to calculate the parameters of the equivalent substrate. We also discussed the R and L extraction under a condition of weak skin effect. The equivalent circuit was validated by comparing its prediction to Q3D and HFSS simulations. Furthermore, the equivalent circuit was verified with measurements on an open terminated structure.

For the FGCPW discussed herein, only the CPW mode was considered in the equivalent model. In reality, the FGCPW has a finite substrate; hence the effects of slab modes, including TE_0 and TM_0 with zero cutoff frequency, can become appreciable. The first substrate mode to start interacting with the CPW is TE_0 [20]. HFSS simulation on the attenuation coefficients α for the CPW and TE_0 mode from 20 GHz to 100 GHz are shown in Figure 15. It is observed that α for both CPW and TE_0 modes become comparable when the frequency exceeds 71 GHz, which indicates the assumption of only quasi-TEM CPW mode propagation in the interconnect is inapplicable at frequencies exceeding 71 GHz. The relationship between TE_0 mode and CPW mode interference at frequencies beyond 71 GHz involves more complicated measurements; this analysis is beyond the scope of this paper.

The equivalent circuit simulation gives a bandwidth higher than 196 GHz; whereas the true bandwidth for the interconnect is set by the frequency at which the quasi-TEM CPW mode no longer dominates. However, despite the overestimated interconnect bandwidth obtained using the equivalent circuit model, we adamantly maintain the model for the FGCPW interconnect is useful for time domain simulations, so long as the quasi-TEM mode is dominant in the interconnect.

REFERENCES

1. Milanović, V., M. Ozgur, D. C. Degroot, J. A. Jargon, M. Gaitan, and M. E. Zaghloul, "Characterization of broad-band transmission for coplanar waveguides on CMOS silicon substrates," *IEEE Trans. Microwave Theory and Techniques*, Vol. 46, No. 5, 632–640, May 1998.
2. Tran, L. N., D. Pasquet, E. Bourdel, and S. Quintanel, "CAD-oriented model of a coplanar line on a silicon substrate including Eddy-current effects and skin effect," *IEEE Trans. Microwave Theory and Techniques*, Vol. 56, No. 3, 663–670, Mar. 2008.
3. Vecchi, F., M. Repossi, W. Eyssa, P. Arcioni, and F. Svelto, "Design of low-loss transmission lines in scaled CMOS by accurate electromagnetic simulations," *IEEE Journal of Solid-State Circuits*, Vol. 44, No. 9, 2605–2615, Sep. 2009.
4. Sayan, A., D. Ritter, and D. Goren, "Compact modeling and comparative analysis of silicon-chip slow-wave transmission lines with slotted bottom metal ground planes," *IEEE Trans. Microwave Theory and Techniques*, Vol. 57, No. 4, 840–847, Apr. 2009.
5. Bénevent, E., B. Viala, and J.-P. Michel, "Analytical modeling of multilayered coplanar waveguides including ferromagnetic thin films on semiconductor substrates," *IEEE Trans. Microwave Theory and Techniques*, Vol. 58, No. 3, 645–650, Mar. 2010.
6. Long, J. R., Y. Zhao, W. Wu, M. Spirito, L. Vero, and E. Gordon, "Passive circuit technologies for mm-wave wireless systems on silicon," *IEEE Trans. Circuit and Systems*, Vol. 59, No. 8, 1680–1693, Aug. 2012.
7. Ansoft HFSS, www.ansys.com.
8. Tsang, L. and X. Chang, "Modeling of vias sharing the same antipad in planar waveguide with boundary integral equation and group T-matrix method," *IEEE Trans. Components, Packaging and Manufacturing Tech.*, Vol. 3, No. 2, 315–327, Feb. 2013.

9. Chang, X. and L. Tsang, "Fast and broadband modeling method for multiple vias with irregular antipad in arbitrarily shaped power/ground planes in 3-D IC and packaging based on generalized foldy-lax Equations," *IEEE Trans. Components, Packaging and Manufacturing Tech.*, Vol. 4, No. 4, 685–696, Apr. 2014.
10. Wu, B. and L. Tsang, "Signal integrity analysis of package and printed board with multiple vias in substrate of layered dielectrics," *IEEE Trans. Advanced Packaging*, Vol. 33, No. 2, May 2010.
11. Hasengawa, H., M. Furukawa, and Hisayoshi, "Properties of microstrip line on Si-SiO_2 system," *IEEE Trans. Microwave Theory and Techniques*, Vol. 19, No. 11, 869–881, Nov. 1971.
12. Shibata, T. and E. Sano, "Characterization of MIS structure coplanar transmission lines for investigation of signal propagation in integrated circuits," *IEEE Trans. Microwave Theory and Techniques*, Vol. 38, No. 7, 881–890, Jul. 1990.
13. Lee, H.-Y. and T. Itoh, "Phenomenological loss equivalent method for planar quasi-TEM transmission line with a thin normal conductor or supperconductor," *IEEE Trans. Microwave Theory and Techniques*, Vol. 37, No. 12, 1904–1909, Dec. 1989.
14. Prodromakis, T. and C. Papavassiliou, "Engineering the Maxwell-Wagner polarization effect," *Applied Surface Science*, Vol. 255, No. 15, 6989–6994, May 2009.
15. Simons, R. N., *Coplanar Waveguide, Circuits,Components, and Systems*, John Wiley and Sons Inc., 2001.
16. Collin, R. E., *Foundations for Microwave Engineering (IEEE Press Serios on Electromagnetics Wave Theory)*, Wiley-IEEE Press, 1992.
17. Heinrich, W., "Quasi-TEM description of MMIC coplanar line including concutor loss effects," *IEEE Trans. Microwave Theory and Techniques*, Vol. 41, No. 1, 45–52, Jul. 1993.
18. Hall, S. H. and H. L. Heck, *Advanced Signal Integrity for High-speed Digital Design*, John Wiley and Sons Inc., 2009.
19. www.ggb.com.
20. Riaziat, M., R. Majidi-Ahy, and I.-J. Feng, "Propagation modes and dispersion characteristics of coplanar waveguides," *IEEE Trans. Microwave Theory and Techniques*, Vol. 38, No. 3, 245–251, Mar. 1990.